A Fast Two-Dimensional Isar-Imaging Process Involving Focusing Techniques

Karl-Heinz Bethke

German Aerospace Research Establishment (DLR)
Institute for High Frequency Technology, D-8031 Oberpfaffenhofen, F.R. Germany

ABSTRACT

A fast process for two-dimensional microwave imaging is presented. A coherent short-pulse radar is used to sample amplitude and phase of the backscattered field from a continuously rotating object while a narrow range gate is swept in range steps of 15 cm across the target plane at a typical speed of 150 m/s. Applying fast synthetic aperture radar (SAR) principles in an off-line process for each range cell, an acceptably good cross-range resolution can be obtained by processing angle intervals of less than 15°. The influence of analytical approximations as well as the effect of range walk can cause severe image degradations. A method for compensation of these effects under the aspect of minimum loss in processing has been developed and will be presented.

INTRODUCTION

Computer aided tomography (CAT) and synthetic aperture radar (SAR) are well known techniques for constructing high resolution microwave images by processing data obtained from different perspective items of a target area. The two-dimensional images provide avaluable insight when diagnosing scattering phenomena by displaying the spatial reflectivity distribution of complex shaped objects. This can clearly highlight scattering features and mechanism or can be utilized as a target identification or classification technique.

Most microwave imaging systems, either commercially available or assembled from laboratory test instruments, can automatically measure the radar cross section RCS of a target in fine frequency increments spanning bandwidths of several GHz. Processing the frequency responses by one-dimensional Fourier transforms results in range resolution along the radar line-of-sight RLS in the order of several centimeters. Due to the limited spatial dimensions of anechoic chambers and the restriction to test- objects of small size, compact ranges are equipped with such systems.

A gated short-pulse radar, however, allows time delay sorting of the echo signals in real time with a high degree of clutter suppression in which case the range resolution is determined by the pulse duration. Pulse durations in the order of 1 ns (equivalent to 1 GHz RF bandwidth) or even less can be realized (Bethke, 1989a, b; Lange, 1991). In many cases a resolution from 15 cm to several meters is sufficient to provide valuable insight when diagnosing scattering phenomena.

Fast imaging techniques are required for time and cost effective investigations of the backscatter behaviour of scale-models or real-world targets. Similarly, airborne intelligence and reconnaissance as well as airport and city traffic surveillance depend on fast imaging techniques, if knowledge of spatial reflector distribution is required for object identification or classification. A coherent short-pulse radar and fast SAR imaging technique provide both measurement and processing speed.

In this paper turntable experiments are studied in which a stationary radar observes a rotating target. Since the relative motion in the inverse case is equivalent, that is by a moving radar and a stationary target as is usual in SAR, SAR imaging can be transferred to ISAR (inverse synthetic aperture radar) imaging and vice versa. A fast SAR technique will be applied directly to small-angle looks to give a two-dimensional reconstruction of the object reflectivity function.

Outdoor experiments will be described which have been conducted with a coherent short-pulse radar. Using 1 ns pulse duration, the range resolution was obtained in real time by stepwise sweeping the delay time of the receiver gate at a considerable velocity while the turget under test was continuously rotated. Image quality degradation which may occur the restriction to one-dimensional fast

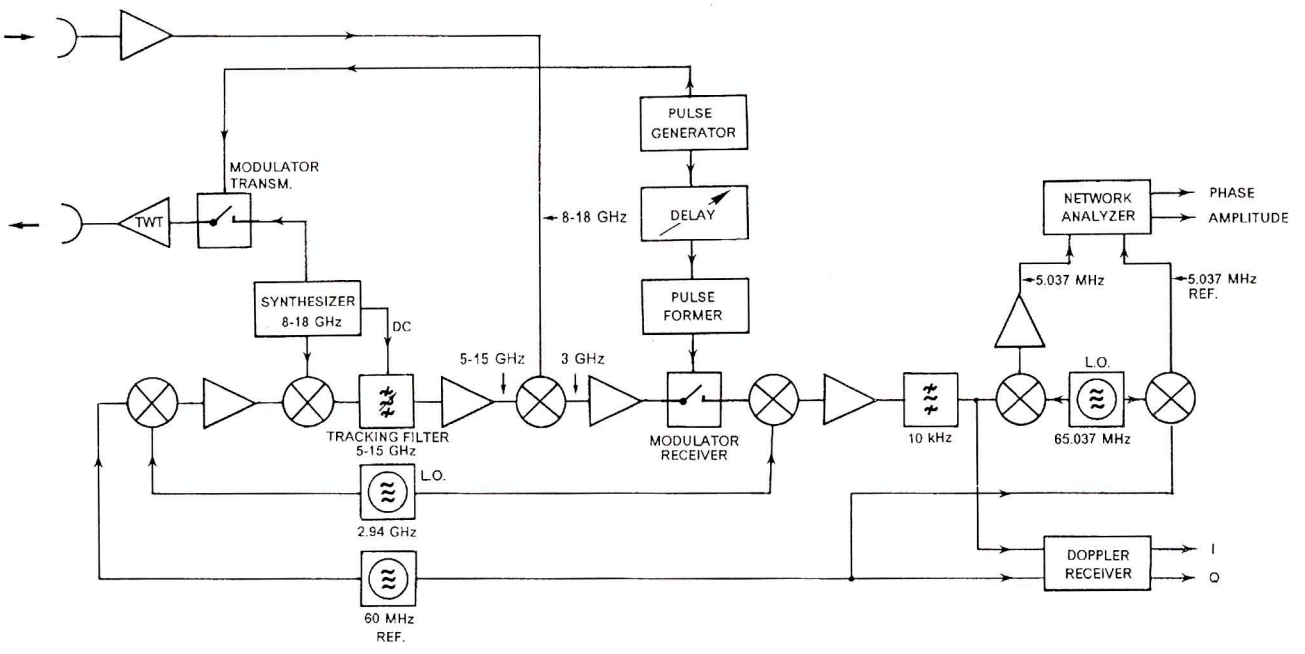

Fig. 1 - Block diagram of the radar system.

Fourier transforms carried out on the content of each range cell will be discussed.

With respect to fast image processing, an effective method for compensating these degrading effects by improved focusing the synthetic aperture will be presented. The focusing process is only applied to time domain raw data which makes possible the use of conventional one-dimensional FFT algorithms.

1. EXPERIMENTAL CONFIGURATION

Experimental data were collected at a fixed frequency using a gated coherent short-pulse radar which covers the frequency range between 8 and 18 GHz. The system was operated with two parabolic reflector antennas, each of 60 cm diameter and a radiated power of approximately 40 W. The receiver gate width as well as the transmitter pulse length is adjustable from 1 μs to 0.8 ns. The delay time for the receiver gate can be linearly swept or, alternatively, digitally swept in minimum increments of 1 ps. This short-pulse radar has been designed for outdoor high resolution RCS measurements of geometric objects, scaled models or real size targets. The applications involve identification of scatterers for target signature definition and modelling, and for RCS reduction. A block diagram of the system is given in Figure 1.

In order to obtain high resolution in range, a constant receiver gate width and transmitter pulse length of about 1 ns were used. In most practical cases this duration is sufficient for studying targets with a maximum cross dimension down to about 1 m. For the purpose of generating microwave images, the delay time for the receiver gate was frequently swept in steps of 1 ns corresponding to range increments of 15 cm. A range increment of less than 15 cm would result in a more finely sampled echo profile, however, the data volume would increase considerably and processing would become much more time consuming. The time period for one range sweep was fixed to 40 ms. Here 40 range steps per sweep starting from a given primary range delay have been programmed which cover a total range depth of 6m containing the target under test. An amplitude and phase (alternatively, in-phase and quadrature component) sampling of the back scattered signal occurs every millesecond.

Most RCS measurements occured at outdoor-ranges suffer from ground reflections. This effect can be suppressed by installing radar fences at proper locations inside the measurement range (Bethke, 1986). Figure 2 shows the typical measurement range for small sized targets as studied in this work.

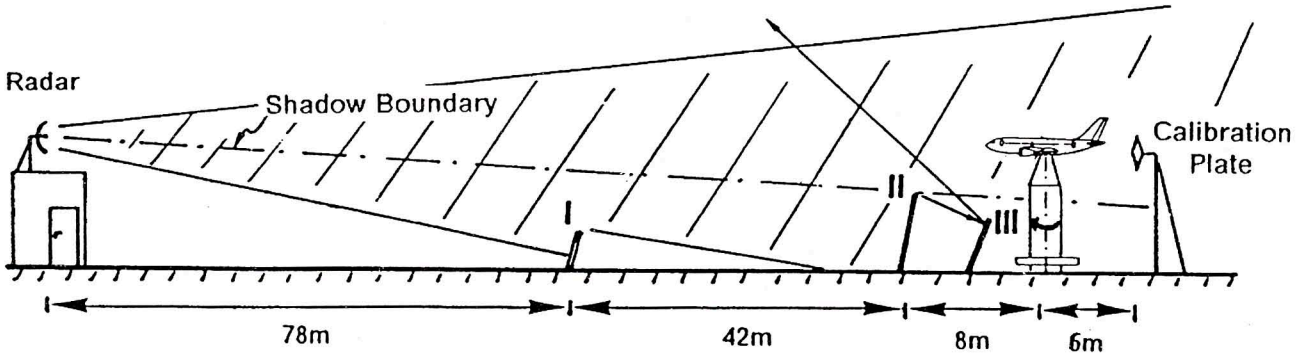

Fig. 2 - Geometry of the outdoor measurement range.

A 1:20 scaled, metalized model of an Airbus A 310 has been mounted on a continuously rotating styrofoam column and is homogeneously illuminated by the stationary radar. An angular encoder connected to the turntable rotator triggers the range gate sweep every 0.1° at a rotational speed of 1°/s. The effective speed of the moving range gate was chosen at 150 m/s, only limited by the given video bandwidth of 3kHz. After one complete object rotation which takes 6 minutes, all required data are available, stored on magnetic tape.

2. FAST IMAGE-PROCESSING

As indicated in the preceding section, the measurement procedure separates the target response into equidistant range cells. Resolution in cross-range is obtained by processing the signal content of each range cell as a function of angular position to extract a Doppler signal which determines the cross-range coordinates with respect to the rotational centre. The value of the reconstructed target reflectivity function $f(x_o, y_o)$ at a position (x_o, y_o) as depicted in Figure 3, is given by the coherent sum of the phase corrected responses $V(x', y', \theta)$ over a finite angular interval (e.g. Bethke, 1989a, b; Mensa, 1991)

$$f(x_0, y_0) = \frac{1}{N} \sum_{n=0}^{N-1} V(x', y', \theta_n) \exp [\, j\varphi (x', y', \theta_n) \,] \qquad (1)$$

where the phase corrections given by the second sum-term eliminate differences in pathlengths existing between the radar sensor and the focused object point at N different aspect angles θ_n. The function $f(x_o, y_o)$ represents an average of the scattering features at the point (x_o, y_o) with respect to the aspect angle. It can only be an approximation of the real object function because the theory adopted here assumes independent and isotropic scattering point sources. Thus, the total signal content in each range cell can be described by linear superposition of all object scattering centres inside a given range cell.

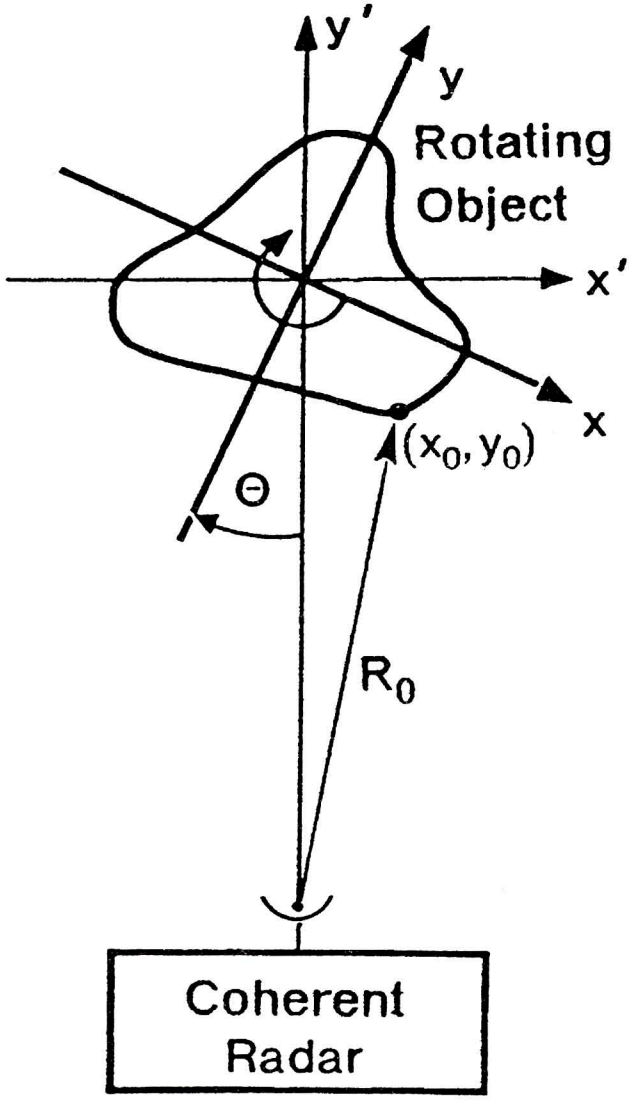

Fig. 3 - Two-dimensional geometry.

Generally, the phase term $\varphi(x', y', \theta_n)$ which is determined by the distance R_o between the radar sensor and the focused object point at (x_o, y_o) is expanded in a series up to linear order assuming that R_o is much greater than $(x_0^2 + y_0^2)^{1/2}$. All aspect angle invariant terms will be neglected. Assuming a clockwise target rotation yields

$$\varphi(x', y', \theta_n) \approx \frac{4\pi}{\lambda}(y_0 \cos\theta_n - x_0 \sin\theta_n)$$

$$\approx -2\pi \frac{2\theta_n}{\lambda} x_0 \; constant \qquad (2)$$

where the phase corrections for small-angle looks, that is $\cos\theta_n \approx 1$ and $\sin\theta_n \approx \theta_n$, are approximately linear in θ and proportional in the cross-range coordinates x_o. Expanding the trigonometric functions in a series up to linear order means that only the movement of a scattering centre in down-range direction causes dominant phase shifts that will be compensated. The beam focusing process includes no phase corrections for a cross-range movement which is determined by second order terms resulting from $y_0 \cos\theta_n$.

According to (1) the result of (2) makes it possible to apply of fast digital Fourier transforms to the signal content of each range-cell in order to steer and focus a narrow synthetic aperture beam across the target plane with minimal computational burden and hence processing time. That provides a two-dimensional image of the projection of the spatial distribution of the scattering centres onto a plane normal to the rotation axis.

After having read the input data, the processing time on a relatively slow μ Vax II computer is in the order of 1.5 seconds for computing an image array of the so-called reflectivity matrix which consists of 128 times 40 complex elements. The operations performed include RCS calibration as well as additional multiplications of the measured respons $V(x', y', \theta_n)$ with a Hamming window in order to reduce the sidelobes of an imaged scattering centre (Bethke, 1989a). On a powerful modern desktop RISC machine this process will only need a fraction of the time mentioned above.

A further important advantage when applying the synthetic aperture principle is the fact that the position of the rotational centre does not have to be known. Therefore, the process described in this paper is suited for imaging of moving targets which also have a translatory velocity component. In this case, an artificial rotational centre is assigned to a selected scattering target point after a prior motion compensation has been performed (Chen, 1980).

In Figure 4 examples of experimental results are shown. The microwave images present the reconstructed object reflectivity of a 1:20 scaled metallized Airbus A 310 under a certain aspect angle and for different polarisations (Bethke, 1991b). Although the pulse length and the range-sweep increment of 15 cm were rather long compared to the maximum object dimension of 2.36 m, the achievable resolution is sufficient in order to identify the different scattering centres. The resolution also permits identification and classification.

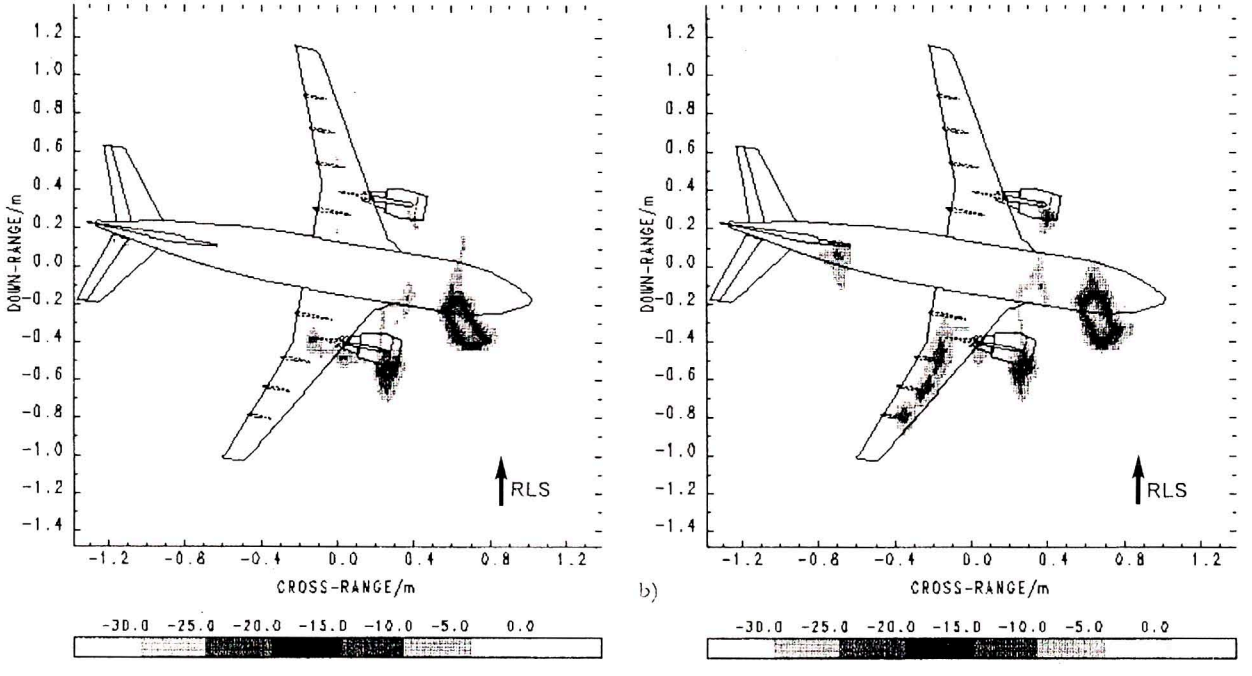

Fig. 4 - Microwave image of a 1:20 scaled Airbus A 310 for; a) horizontal; b) vertical polarisation; frequency 12.5 GHz; process angle 12.8°, range resolution 15 cm, RCS in dBsqm.

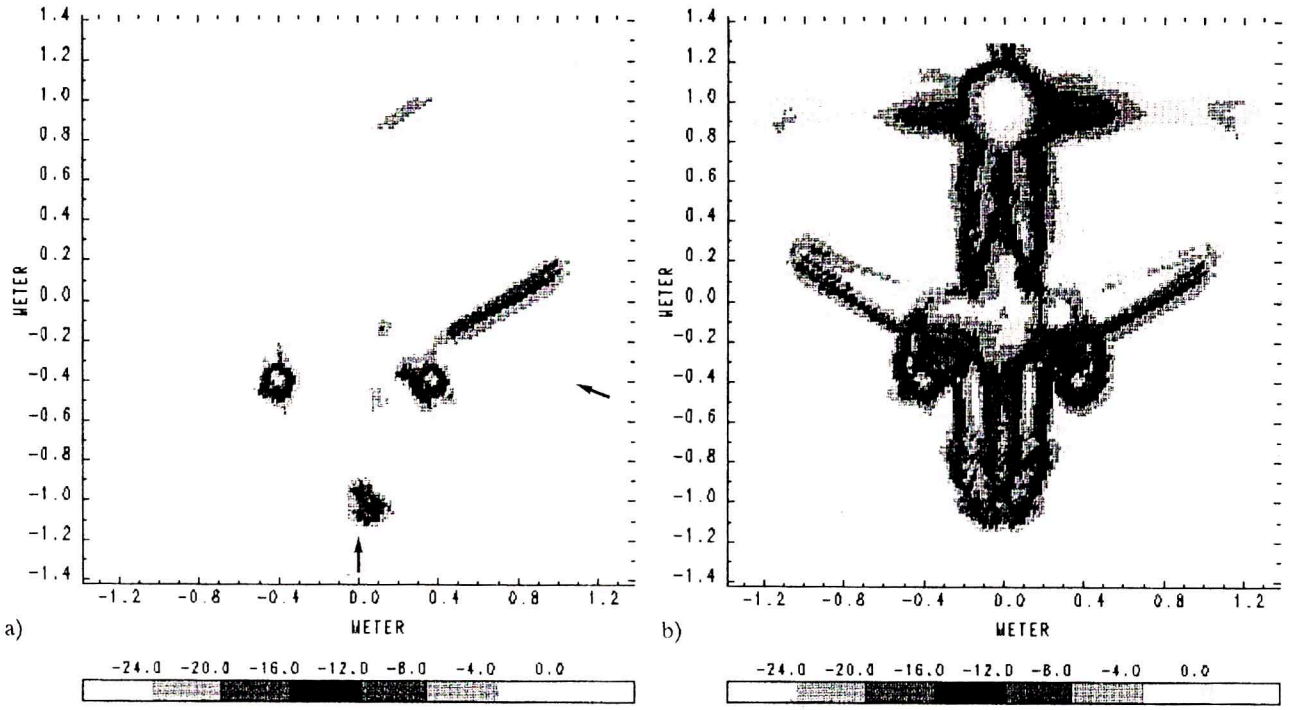

Fig. 5 - Image reconstructed by incoherent superposition of; a) 29 looks according to a 70° - view; b) 144 looks according to a 360° - view.

A noncoherent superposition of several processed narrow-angle looks, where only the maximum amplitude value is taken into account, gives a more complete representation of the reflectivity function. Figure 5a shows the result after superimposing 29 looks covering a total aspect angle of 70°. Dominant echo contributions from the turbines, wings and fuselage can be identified which, e.g., would contain enough information for a classification. In Figure 5b the total object reflectivity is shown reconstructed from 144 looks.

3. IMAGE DEGRADING EFFECT

The image process presented here may suffer from two degrading effects if high resolution is desired. A wide range of aspect angles is required for a fine cross-range resolution which is determined by the cross-range cell size Δx via the relation

$$\Delta x = \frac{\lambda}{2\,\Delta\theta} \quad ,$$

$\Delta\theta$ = process angle (range of aspect angles).

The approximations applied may no longer hold at the outer bounds of the image plane.

Degradations in down-range mainly result from the approximation $y \cdot \cos\theta \approx constant$ by which the phase corrections in (1) do not account for migrations through cross-range resolution cells. From the results in (Bethke, 1989a, b) one finds that the approximations are quite good if the maximum phase error meets the condition

$$\frac{4\pi}{\lambda} y_i\,(1 - \cos\Delta\theta/2) \lesssim \pi \,. \qquad (4)$$

Assuming equal lengths of transmitter pulse and receiver gate, the maximum amplitude decrease in down-range will be less than about 4 dB when using a rectangular window and less than about 1.5 dB when using a Hamming window. In addition, no blurring along the down-range coordinate will appear.

The second and most severe degrading effect on image quality is caused by the migration of a scattering centre through more than one range cell during the process angular interval $\Delta\theta$. The so-called range walk reduces the effective width of the synthetic aperture and hence the resolution capability.

Since the convolution of two equal sized rectangular functions of width Δy yields a triangular function of width $y_{conv} = 2\,\Delta y$, the response of a scattering centre that migrates through a range cell during the process angle interval will be weighted by this triangular function of the range gate. Figure 6 shows different cases for the simulated response $|\,V(x', y', \theta_n)\,|$ of a point reflector moving on circles of different radii. Depending on its cross distance, it migrates through up to 5 range cells during $\Delta\,\theta$. Here, a convolution interval of $y_{conv} = 2.6\,\Delta y$ (Δy = pulse length and range sweep increment)is assumed, accounting for nonideal rectangular pulse shapes. From Figure 6 it can be seen that for large cross distances the interval for a measurable response will become shorter than the total process interval. At the same time, contributions of the scattering point will appear in several cells neighbouring the i-th range cell. Thus, the range walk may cause blurring characterized by an amplitude decrease of the reconstructed average reflectivity function, by a decrease in range resolution and according to (3) by a decrease in cross-range resolution.

Meeting the condition

$$|\,x\,| \cdot \Delta\,\theta < y_{conv} \qquad (5)$$

where $|\,x\,|$ denotes the maximum cross distance of a target point will keep image degradations at the outer bounds of the image plane at a tolerable level. From the results in (Bethke, 1989a, b) one can find that no significant blurring will appear and that the maximum amplitude degradation in cross-range will be less than 7 dB for rectangular weighting and less than 4 dB when using a Hamming window.

For the microwave images in Figures 4 and 5 the parameter choice meets conditions (4) and (5) so that only small degradations of image quality may appear at the outer image bounds. However, without meeting conditions (4) and (5) a reduced resolution has to be expected.

4. CORRECT FOCUSING IN THE TIME DOMAIN

Focused microwave imaging has to account for the migration paths of target scattering centres during the processing interval. Generally, this is solved by swept or stepped frequency measurements. The desired phase corrections are already accomplished in the frequency domain. Transformation into the time domain then yields a focused image. These techniques are known as polar format processing (e.g. Walker, 1980; Mensa, 1991) or computer tomography (e.g. Hermann, 1979; Fuchs, 1990).

When measuring in the time domain the signal of a scatterer moving through a costant range cell may be angularly limited which prevents correct focusing. A possible way to avoid this limitation would be Fourier transforming of time domain data into the frequency domain, then applying the desired phase corrections and finally transforming the result back into the time domain which results into a correct, focused image (e.g. Brown, 1969; Kleintz 1991). Such methods, however, involve considerable computational effort and hence processing time. In addition, loss in resolution is to be expected due to the multiple transformation of windowed data.

In order to realize a correct focusing of the synthetic aperture in the time domain two conditions have to be met: taking into account higher order terms and the assurance of a function $V(x', y', \theta_n)$ that is nearly independent of the range walk.

According to (2), phase corrections including higher order terms are easily accomplished by simply adding a phase contribution to the phase of each measured signal response per range cell which is defined by $(4\pi/\lambda) \cdot y_0 \cos\theta_n$.

For compensation of the range walk, the function $V(x', y', \theta_n)$ of a given range cell has to be reorganized along the process interval $\Delta\,\theta$. A scattering centre migrating through a given range cell only yields a maximal signal response along a fraction of the total interval $\Delta\,\theta$ where correct focusing is possible. At other process angles this scattering centre will appear in neighbouring range cells as is demonstrated in Figure 6.

Therefore, the original angular interval can be divided into subinterval contains the signal response of the actual range cell in which the maximum signal just appeares. In Figure 6 these subintervals are characterized by the dashed angular regions. The subinterval length depends on the lateral location x to which the synthetic aperture beam is steered, on the range gate function, on the range increment $\Delta\,y$ and, of course, on the total process angle $\Delta\,\theta$.

The reorganization of the original signal response in a given range cell tracks a scattering centre in down-range so that the synthetic aperture now can be correctly focused. Using this concept, it is possible to find a more detailed reorganization scheme which forms a signal response with nearly constant amplitude along the processing interval (Bethke, 1991a).

Applying this tracking technique at each step of steering the focused beam will require much more computer time, because fast FFT algortihms can not be used for this direct

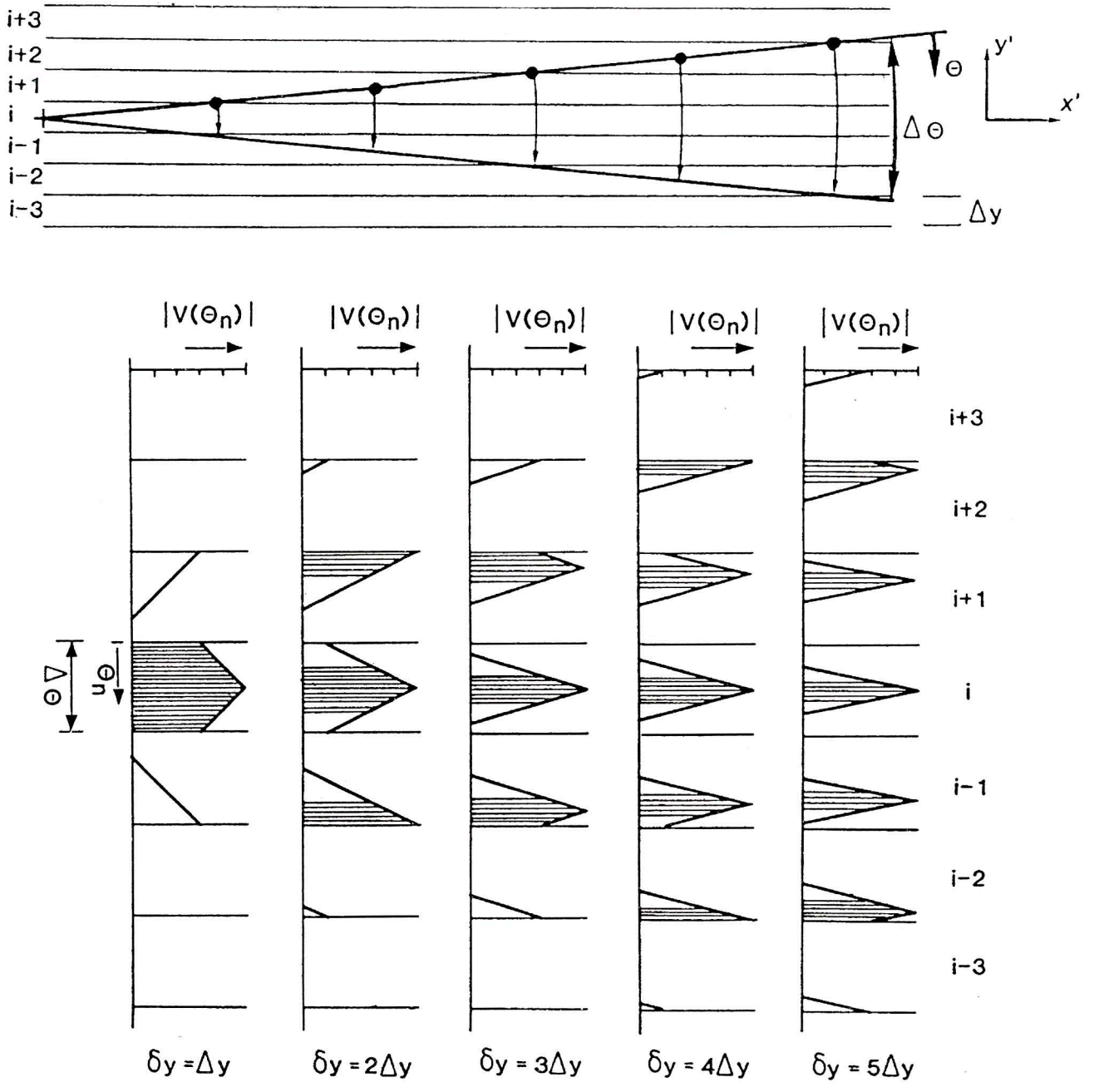

Fig. 6 - Different cases of rage walk: simulated signal responses in the i-th range cell and its neighbour-cells shown for a point scatterer moving on circles of different radii. During the proces interval Δ θ the point scatterer covers the distances δ y in range (Δ y = range cell width). The dashed regions characterize angular subintervals which are used to form an individual, focused synthetic aperture in the i-th range cell (see section 5).

method. Therefore, in cross-range direction the image plane is divided into strips running parallel to the range coordinate. Referred to the lateral centre of each strip, an individual tracking procedure is applied which only depends on the cross distance of the strip centre and which does not depend on the range cell position relative to the rational centre.

Inside each strip this procedure results in an optimally focused aperture for a point reflector at the strip centre. If the cross-range extension of a strip is dimensioned such, that differences in range walk inside each strip remain small, then for every position inside a given strip a common tracking procedure for the strip centre will approximately hold (Bethke, 1991a). Consequently, FFT algortihms can be applied again to generate an optimally focuse dimage around each strip centre. Only the reconstructed reflectivity function inside each strip is taken into account to construct the final image.

The increase in computational effort for this focusing method varies with the number of strips. The number of strips depends on the maximum object dimension, the range gate increment (which here corresponds to the pulse length) and values given above, the definition

$$x_m = (m + 0.5)\frac{\Delta y}{\Delta \theta}\ , \quad m = 1,2,3,\ldots \tag{6}$$

has been found useful, where $\pm x_m$ denotes the boundaries of the strips in cross-range direction. In practice more than 5 different strips are rare so that the computational time will not exceed the original computational time by more than half an order.

Figure 7 gives an example for the efficiency of this method. In an experiment three biconical reflectors were moved on circles with a medium radius of about 1 m. In order to generate a considerable range walk, the images were processed with an unusually large angular interval of 51.2° whereby a maximum migration path for the outer reflector through more than 6 range cells was realized.

A further example is given in Figure 8 where the Airbus model is imaged using the same process angle. If no focusing techniques are applied, heavy blurring will distort the microwave image. It is noted that the image resolution in the examples of Figures 7 and 8 is not well proportioned, because the down-range resolution given by the range gate was fixed. For instance, in Figure 8 the cross-tange cell size is 1.3 cm while in down-range the cell size is 15 cm which results in unproportioned pixel contour plots.

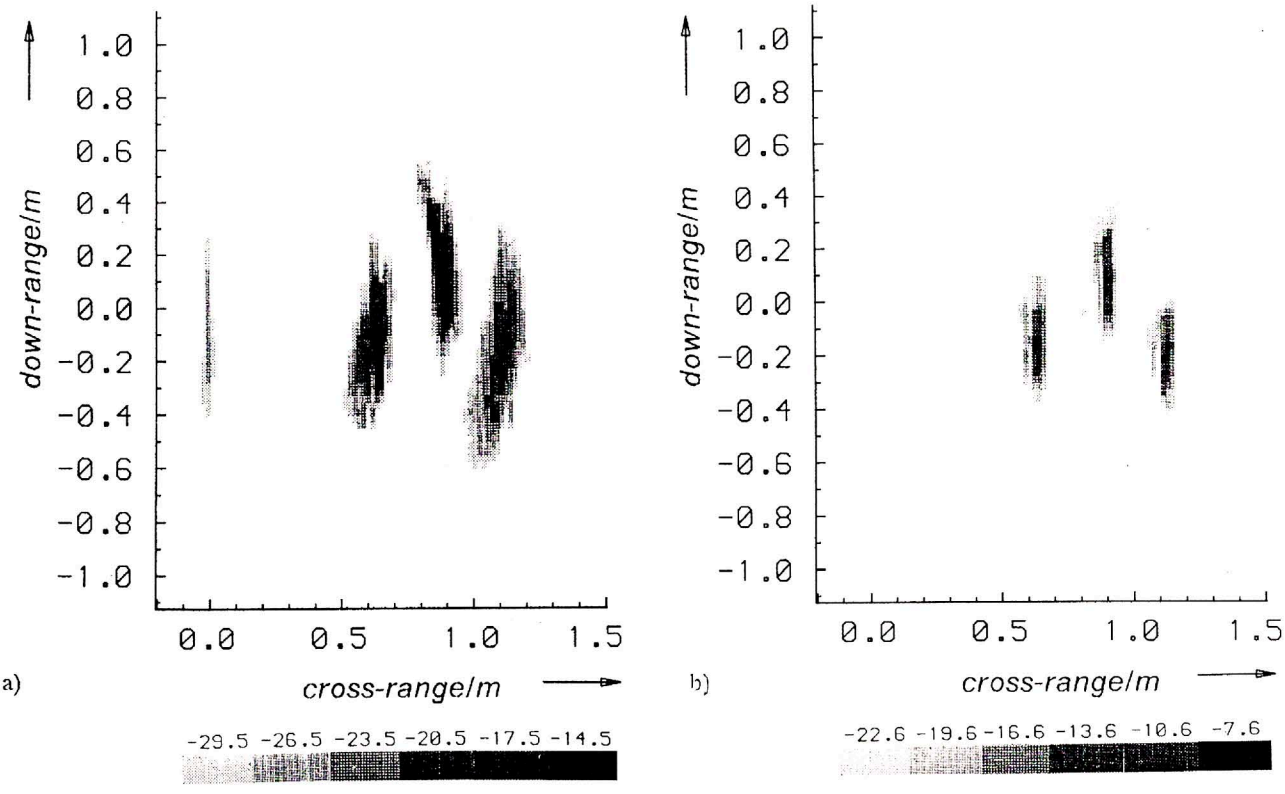

Fig. 7 - Image of three biconical reflectors; a) result from an ill focused aperture; b) correctly focused image constructed from fosuced subimages; frequency 10.0 GHz, process angle 51.2°, range resolution 15 cm.

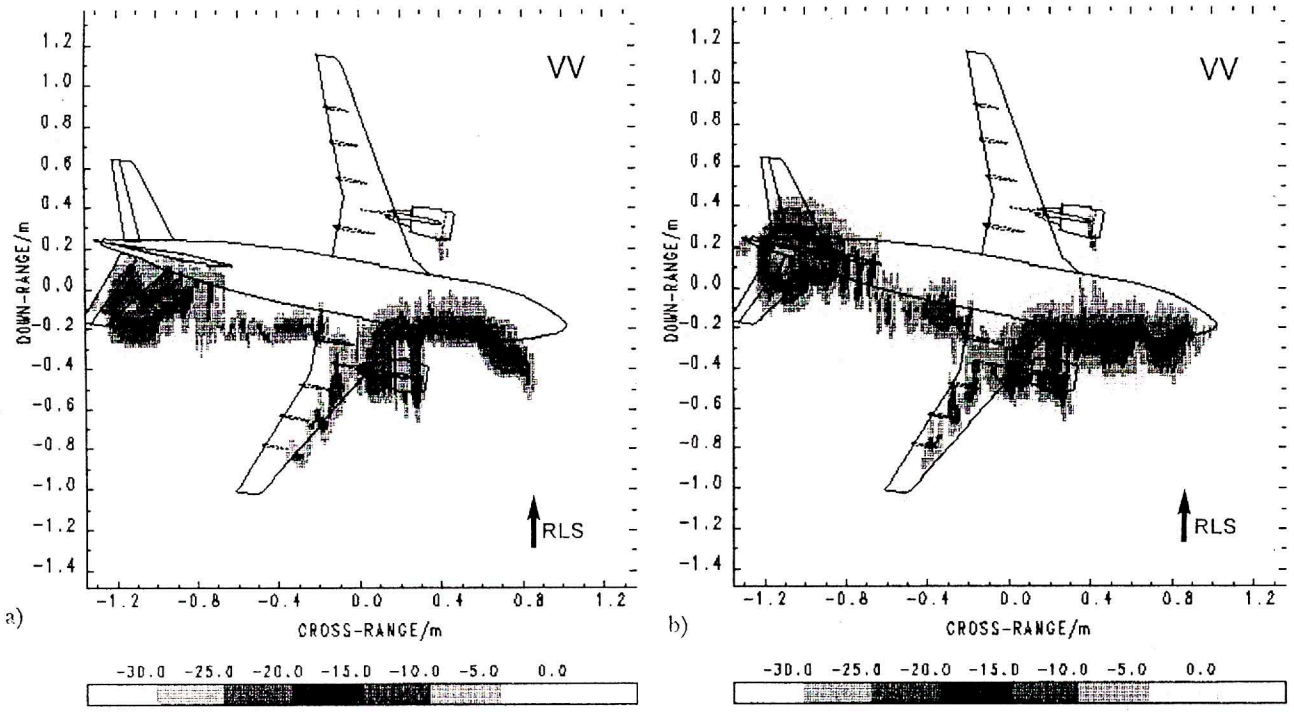

Fig. 8 - Imaged Airbus model; a) result from an ill focused aperture; b) correcty focused image constructed from focused subimages; frequency 12.5 GHz, process angle 51.2°, range solution 15 cm.

Overall, it can be stated that the additional time for generating correctly focused images can be held at a tolerable level with respect to a fast imaging process. Further more, a correctly focused aperture obtained by processing pure time domain raw data requies no data manipulations with inherently unknown effects as they may occur with methods that require additional forward and backfward transformations of windowed data.

CONCLUSION

In this paper a combined hardware/software method for generating fast two-dimensional ISAR images has been presented. The one-dimensional RCS-profiles versus range are produced in real time with the aid of a gated coherent short-pulse radar. Small-angle looks are sufficient to obtain high cross-range resolution using fast SAR principles.

Incorrect focusing of the synthetic aperture may cause severe degradations to image quality. The main mechanism for these effects have been identified. Taking higher order phase terms into account and applying an individual tracking procedure with respect to the migration paths of scattering centres along the down-range coordinate will give focused image strips which are combined to result in a final correctly focused image with a tolerable amount of computational effort and processing time. Examples of processed images from experimental data demonstrate the capabilities of the fast synthetic aperture principle.

REFERENCES

Bethke K,H., 1986, Investigation of Signal Degradation by Scattering and its Suppression in Near-Ground Radar Cross-Section Measurements. Final Report, ESA-TT-967, German Aerospace Research Establishment, Oberpfaffenhofen. Translation of DFVLR-FB-85-42, Untersuchungen zur Stoerstreuung und Methoden zu deren Unterdrueckung bei bodennahen Radarrueckstrahlmessungen.

Bethke H.K., 1989a, On a Fast Two-Dimensional Radar Imaging process for Rotating Targets and an Analysis of its Image Quality. Final Report, ESA-TT-1142, German Aerospace Research Establishment, Oberpfaffenhofen. Translation of DFVLR-FB-88-51, Ein schnelles zweidimensionales Radarabbildungsverfahren fuer rotierende und eine Analyse der Abbildungsqualitaet.

Bethke K.H.; Roede B., 1989b, A Fast ISAR-Imaging Process and its Inherent Degrading Effect on Image Quality, AGARD-CP-359, High Resolution Air- and Spaceborne Radar, 31-1.

Bethke K.H., 1991a Fokussierte zwedimensionale Radarabbildung durch koarente Signalverarbeitung im Zeitbereich. Final Report, DLR-FB-91-19, German Aerospace Research Establishment, Oberpfaffenhofen.

Bethke K.H., 1991b, Globale und hochaufgeloeste Radarrueckstrahlquerschnitts-Messungen und zweidimensionale Mikrowellenabbildungen von einem skalierten Flugzeugmodell vom Typ Airbus A 310. Communication, DLR-Mitt.91-10, German Awrospace Research Establishment, Oberpfaffenhofen.

Brown W.M.; Fredericks R.J., 1969, Range-Doppler Imaging with Motion Through Resolution Cells. IEEE AES-5, 1, 98.

Chen C.C.; Andrews H.C., 1980, Target-Motion-Induced Radar Imaging. IEEE AES-16, 1, 2.

Fuchs U., 1990, Streuzentrnanalyse in der Mikrowellenabbildung einfacher metallischer Koerper. Final Report, DLR-FB- 90-32, German Aerospace Research Establishment, Oberpfaffenhofen.

Hermann G.T., 1979, Image Reconstruction from Projections. (Boston, London: Springer Verlag).

Kleintz M., 1991, Focussed Mono- and Bistatic Range-Doppler-Imaging of Rotating Targets with a Coherent Pulse Radar. This issue.

Lange M.; Detlefsen J., 1991, 94 GHz Three-Dimensional Imaging Radar Sensor for Autonomous Vehicles. IEEE MTT-39, 5, 819.

Mensa D.L., 1991 High Resolution Radar Cross Section Imaging. Bboston, London: Artech House).

Walker J.L., 1980, Range-Doppler Imaging of Rotating Objects. IEEE AES-16, 1, 23.